Highlights

Experimental Validation of Corrugated Surface Profiles for Multipactor Mitigation in Gap Waveguide Technology

S. M. Bonte, A. Coves, A. A. San-Blas, J. J. Vague, V. E. Boria

- A corrugated surface profile is experimentally demonstrated to mitigate the multipactor effect in gap waveguide microwave circuits
- A parametric study of the influence of the number of corrugations is performed
- A significant increase of the multipactor power threshold is achieved in a ridge gap waveguide section and in a groove gap waveguide bandpass filter

Experimental Validation of Corrugated Surface Profiles for Multipactor Mitigation in Gap Waveguide Technology*

S. M. Bonte[a], A. Coves[a,*], A. A. San-Blas[a], J. J. Vague[b] and V. E. Boria[b]

[a]Department of Communications Engineering-I3E, Miguel Hernández University of Elche, Elche, Spain
[b]Department of Communications-iTEAM, Technical University of Valencia, Valencia, Spain

ARTICLE INFO

Keywords:
gap waveguide technology
microwave
multipactor mitigation

ABSTRACT

This work presents the design, fabrication, and experimental validation of corrugated surface profiles to mitigate the multipactor effect in gap waveguide technology. Two representative structures —a ridge gap waveguide (RGW) section and a groove gap waveguide (GGW) bandpass filter— are investigated. Corrugations are introduced in regions of maximum electric field to disrupt electron trajectories and increase the multipactor threshold power. A comprehensive study combining full-wave electromagnetic simulations and particle tracking is carried out to evaluate their impact on RF performance and multipactor susceptibility. Different corrugation configurations are assessed to achieve an optimal trade-off between improved power-handling capability and minimal electrical degradation. Prototypes are manufactured using standard CNC milling and experimentally tested under high-power vacuum conditions. Results show a significant increase in multipactor threshold power (about 1.5–2 kW) in both RGW and GGW structures, while maintaining low insertion loss and high return loss. The good agreement between simulations and measurements confirms the effectiveness of this simple, passive, and effective solution for enhancing the power-handling capability of gap waveguide components. The main contribution of this work is the application of corrugated profiles for multipactor mitigation, along with its experimental validation using practical RGW and GGW components.

1. Introduction

Multipactor (MP) is a well-known high-power breakdown phenomenon that occurs in microwave and millimeter-wave components operating under vacuum conditions, where free electrons are accelerated by radio-frequency (RF) electromagnetic (EM) fields and generate secondary electron emission upon impact with metallic surfaces. This resonant electron multiplication process can lead to severe degradation of system performance, including increased noise, detuning of resonant structures, and even irreversible physical damage [1]. The fundamental mechanisms governing multipactor discharges were first described in classical works such as [2, 3, 4], and later expanded through experimental and theoretical investigations focused on RF systems [5, 6]. Over the past decades, extensive research has been devoted to understanding multipactor behavior in conventional transmission lines and waveguide technologies, including rectangular, coaxial, and ridged structures [7, 8]. In parallel, several experimental studies have provided multipactor threshold levels in practical components and materials, confirming their strong dependence on geometry, frequency, and secondary electron emission properties [9, 10]. These works highlight the importance of accurate prediction and mitigation strategies for ensuring reliable operation in high-power environments, particularly in space applications where vacuum conditions are inherent. It has also been reported that relatively small variations in SEY parameters, caused by handling, contamination, or surface preparation conditions, can significantly affect predicted multipactor thresholds [11].

More recently, gap waveguide (GW) technology has emerged as a highly attractive alternative for high-frequency applications due to its low-loss characteristics, relaxed electrical contact requirements, and compatibility with standard manufacturing processes. Among its different implementations, ridge gap waveguide (RGW) and groove gap waveguide (GGW) structures have demonstrated excellent performance in filters, transmission lines, and antenna feeding networks. However, previous investigations have shown that these technologies may still be susceptible to

* This work has been funded by the Ministerio de Ciencia, Innovación y Universidades (Spanish Government) through the Subprojects C41 and C43 of the R&D Project PID2022-136590OB and by European Social Fund+ (ESF+).

*Corresponding author
angela.coves@umh.es (A. Coves)
ORCID(s): 0000-0003-1917-8661 (A. Coves)

multipactor discharges due to the presence of critical regions with high electric field concentration and small effective gaps [12, 13]. To address this issue, different mitigation techniques have been proposed in the literature. These include the use of surface coatings with reduced secondary electron yield (SEY) [14, 15], engineered geometries to redistribute EM fields [16], and dedicated suppression devices [17, 18]. Although these approaches can be effective, they often introduce additional fabrication complexity, cost, or reliability concerns, particularly in space-qualified hardware.

In this context, surface texturing techniques have gained increasing attention as a passive and manufacturable solution for multipactor mitigation. Among them, the introduction of corrugated surface profiles has recently been proposed as an effective method to disrupt resonant electron trajectories, and reduce the probability of sustained electron multiplication [19, 20]. In a recent study, it was demonstrated, through numerical simulations, that corrugations applied to critical regions of microwave filters can significantly increase the multipactor power threshold, while preserving the RF response of the component [21]. The effectiveness of this approach lies in its ability to modify the local EM boundary conditions and electron impact dynamics without requiring additional materials or coatings. Despite these promising results, most of the work reported so far has been limited to numerical analysis, and experimental validation in practical gap waveguide components remains scarce. In particular, there is a lack of comprehensive studies combining simulation and high-power measurements to assess the effectiveness of corrugated surfaces in realistic GW structures, such as RGW and GGW devices.

Building upon previous works on multipactor characterization in GW technology [10, 12], this paper presents a systematic investigation of corrugated surface profiles applied to two representative components: a RGW transformer and a GGW bandpass filter operating in the Ka-band. Both structures were previously designed, fabricated and experimentally characterized in terms of RF response and multipactor threshold power, providing a reliable reference baseline for comparison.

Although the technique presented in this paper is applied to GW technology in the Ka-band frequency range, it is important to note that the same approach has previously been demonstrated for other waveguide-based components, including a rectangular waveguide section and third- and fifth-order interdigital filters [21], operating at different frequency ranges. Therefore, the proposed methodology is not limited to GW technology or the Ka-band and can be readily extended to a wide range of waveguide components and frequency bands.

In this new contribution, corrugations are introduced in the metallic top lid of both devices, specifically in the regions where the electric field reaches its maximum value —namely, above the ridge in the RGW and at the central cavity of the GGW filter. A detailed simulation campaign is carried out using full-wave EM solvers in combination with electron-tracking tools, to evaluate the influence of the corrugation geometry and the number of inserted corrugations on both RF performance and multipactor behavior. The proposed solutions have been manufactured using standard CNC milling techniques, and experimentally validated through high-power multipactor testing under vacuum conditions in a dedicated RF facility. The main objective of this work is to demonstrate, through both simulations and measurements, that corrugated surfaces provide a simple, passive, and effective solution to significantly enhance the multipactor threshold power in gap waveguide technology, while preserving the excellent RF characteristics of the original designs.

2. Corrugated surface profile: concept and design

In a previous study [21], the implementation of corrugated surface profiles was demonstrated to be an effective technique to enhance the power-handling capability of microwave components affected by multipactor. In particular, corrugations with a triangular profile exhibit a higher mitigation of the multipactor effect, as discussed in [21]. In order to implement such triangular profiles in practice, milling techniques are required.

Based on preliminary simulations, a corrugation depth of $h_{\mathrm{corr}} = 100\ \mu$m was selected (see Fig. 1), as it provides a significant increase in the MP threshold power (P_{th}) without degrading the RF performance. Additionally, as shown in Fig. 1, a small chamfer (of 3 μm in this case) has been included in the simulations at the peaks and valleys of the corrugations, in order to avoid problems associated with the meshing and convergence in such regions, and considering that the corrugations are not expected to be perfectly sharp in practice.

From a manufacturing point of view, the milling tool imposes a cutting angle of 60°. Therefore, the corrugation width w_{corr} can be derived as:

$$\tan(30°) = \frac{x}{h_{\mathrm{corr}}}, \quad x = h_{\mathrm{corr}} \cdot \tan(30°), \tag{1}$$

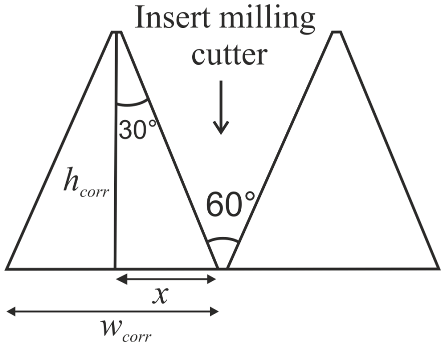

Figure 1: Scheme and relevant dimensions in a triangular corrugated profile.

Table 1
Design parameters of the RGW prototype (all values in mm)

a_{ridge}	h_{ridge}	H_A	p	d	a_{pin}	h_{pin}	H_{gap}	H_{G}
3	5.75	1.1	1.1625	3.25	1.5	5.75	0.727	6.85

$$w_{corr} = 2x \approx 115\ \mu\text{m}. \tag{2}$$

These dimensions were used for all corrugated lids (triangular profile) implemented in this work.

3. Designs With Corrugations: Simulation Results

Two GW structures were selected to experimentally validate the proposed corrugated surface profile theory: a RGW transformer and a GGW bandpass filter. Both components were designed, manufactured and experimentally characterized in previous works (see [10] for the GGW filter and [12] for the RGW transformer) without considering the inclusion of corrugations. For both designs, in this section we analyze the effect of introducing different numbers of corrugations on the top lid of each component to assess the influence of the corrugated surface profile on both their power-handling capability (P_{th}) and their RF performance. To maximize their impact, the corrugations have been placed in the region of highest electric field intensity, which is located at the center of both structures. Consequently, the corrugations have been positioned over the ridge in the RGW configuration and over the groove in the GGW configuration.

3.1. Analysis of the P_{th} in a corrugated RGW transformer

The analyzed RGW transformer was originally studied in [12]. The structure consists of an E-plane WR-51 waveguide transformer, where the central section is implemented in RGW and whose central ridge is surrounded by a periodic bed of metallic pins, which creates a high-impedance boundary. Fig. 2 shows the geometry of the RGW transformer under study, while the values of the different parameters are reported in Table 1.

The design is intended for Ka-band operation, and selected to match the available RF power at the high-power facility (where the MP tests will be carried out) of the European Space Agency operated in collaboration with the Val Space Consortium [22], while ensuring that the obtained multipactor results remain scalable to higher-frequency implementations of RGW technology. The design required the use of full-wave EM simulation tools, including the high-frequency solver of CST Studio Suite [23] together with its electron-tracking code (Spark3D module). The resulting fields within the operating band were exported to Spark3D to evaluate the power threshold, and establish a reference baseline prior to introducing the corrugated surface to the top lid. For this design, simulations are carried out for three frequencies in the operational band: 17 GHz, 17.4 GHz and 18 GHz.

In the simulations, the initial number of electrons was set to 10,000, and they were uniformly distributed over the full simulation region to avoid preferential triggering of the discharge in localized areas. The multipactor detection criterion was defined using the default settings of the simulation software. After validating the RF matching, the EM

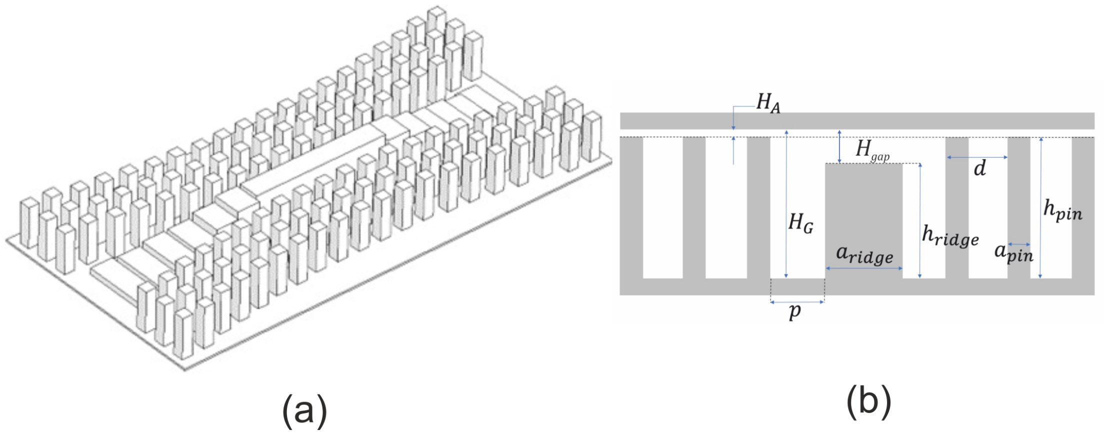

Figure 2: (a) 3D view of the RGW transformer. (b) Cross section of the RGW.

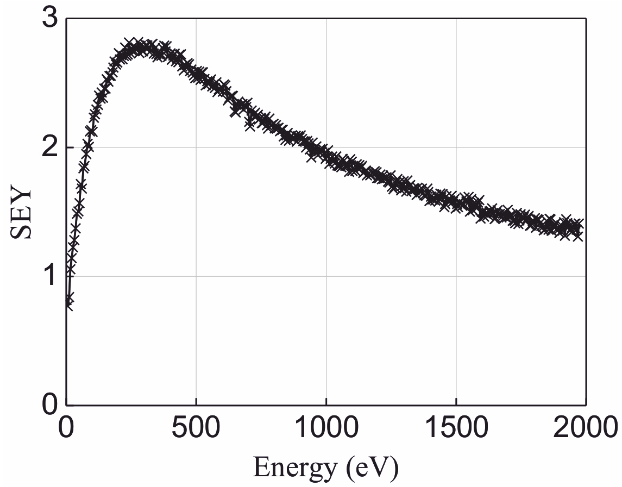

Figure 3: Experimental SEY of the aluminum material used in the fabrication of the RGW transformer [12].

Table 2
SEY data for aluminium (Al) material

Material	E_{max} (eV)	E_1 (eV)	δ_0	δ_{max}
ECSS2020 [24]	276.0	17.0	0.8	2.92
Measured SEY in [10]	246.5	16.154	0.903	2.485

field distribution in the transformer was exported to Spark3D, where multipactor simulations were performed using the previously defined parameters and two different SEY values. On the one hand, the measured SEY values of the aluminum material used in the fabrication of the RGW transformer [12] shown in Fig. 3 and, on the other hand, the European Cooperation for Space Standardization (ECSS) standard SEY value for aluminum (see Table 2).

In order to choose the number of corrugations we want to implement on the top lid of this RGW design, a study was conducted to evaluate the influence of the number of inserted corrugations on both the MP power threshold level and the RF performance of the considered example. In Table 3, the simulated P_{th} values obtained using the experimental SEY of Fig. 3 for several number of corrugations are shown, while Table 4 shows those obtained using the ECSS SEY.

The results reported in Tables 3 and 4 clearly show that increasing the number of corrugations leads to a significant increase in P_{th}. Furthermore, RF performance has also been verified to not be significantly degraded by the introduction

Table 3
Simulated P_{th} values for RGW with experimental SEY

Design	17 GHz	17.4 GHz	18 GHz
Smooth lid	3593 W	3743 W	4056 W
15 corrugations	5937 W	6234 W	6812 W
20 corrugations	7452 W	8015 W	8432 W
30 corrugations	8343 W	8155 W	8781 W

Table 4
Simulated P_{th} values for RGW with ECSS SEY

Design	17 GHz	17.4 GHz	18 GHz
Smooth lid	3351 W	3585 W	3820 W
15 corrugations	5296 W	5671 W	5952 W
20 corrugations	7077 W	7440 W	7546 W
30 corrugations	7312 W	7921 W	8062 W

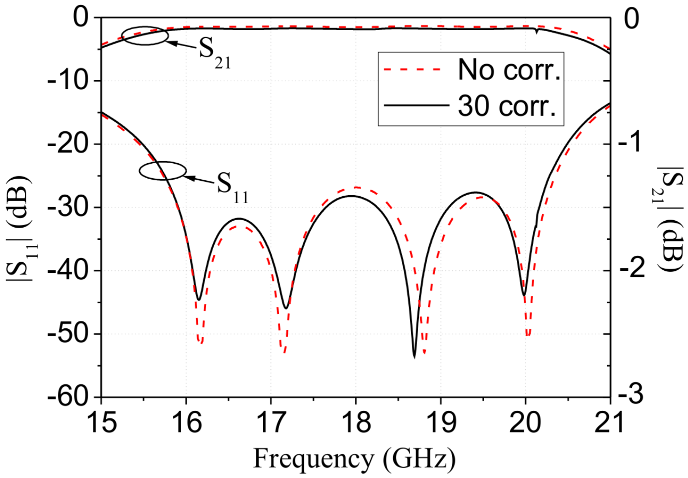

Figure 4: RF performance of the RGW transformer with smooth lid and with 30 corrugations.

of corrugations, as shown in Fig. 4, where the electrical response of the RGW with a smooth lid and with the maximum number of corrugations (30) is compared, revealing that the introduction of corrugations has a negligible impact on insertion and return loss.

Taking into account the power limitations of the available high-power test facility (about 6 kW), a configuration with 15 corrugations was selected for fabrication, in order to have clear experimental evidence of good RF performance with a significant number of corrugations. With this configuration, although only a MP discharge is expected to be detected at 17 GHz, the improvement in terms of increase of P_{th} can be scaled to higher frequencies according to Tables 3 or 4. Fig. 5 shows the final corrugated lid with 15 corrugations, longitudinally along the RGW axis and centered on the top lid, where the electric field reaches its maximum value. The corrugated section is terminated 9.75 mm from each port (excluding the final step) to preserve field stability.

3.2. Analysis of the P_{th} in a corrugated GGW bandpass filter

The GGW bandpass filter analyzed in this section (originally designed in [10]), was intended to operate at Ka-band. It consists of inductively coupled cavities implemented in groove gap waveguide technology, whose 3D view and cross section are shown in Fig. 6. Furthermore, the values of the different parameters of the GGW filter stated in Fig. 6(b) are shown in Table 5.

Figure 5: Corrugated top lid for the RGW transformer. (a) 3D view. (b) Front view.

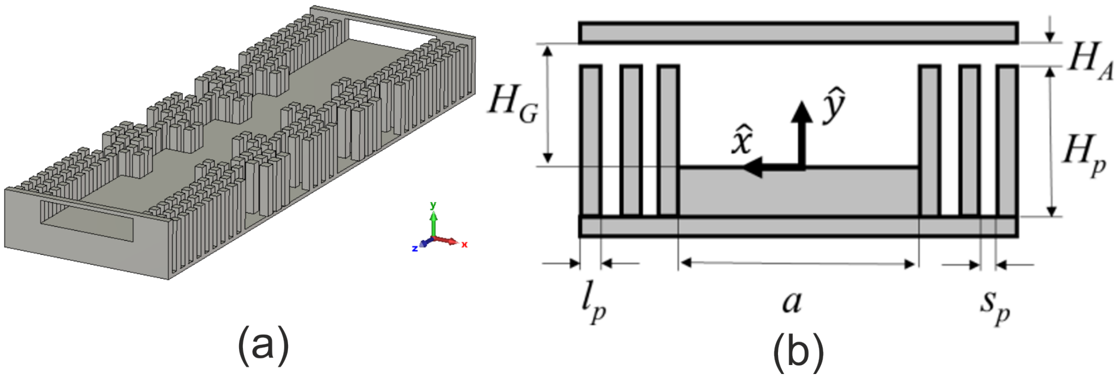

Figure 6: (a) 3D view of the inductive bandpass filter in GGW technology. (b) Cross section of the GGW.

Table 5
Design parameters of the GGW filter

s_p	l_p	H_G	a	H_p	H_A
0.96 mm	1.02 mm	3 mm	12.954 mm	6.477 mm	20 μm

Table 6
Simulated P_{th} values for the GGW filter

Design	Measured SEY	ECSS SEY
Smooth lid	3679 W	3164 W
20 corrugations	5562 W	6047 W
25 corrugations	5937 W	6140 W
30 corrugations	7171 W	6515 W

The EM field distribution in this filter, computed with CST Studio Suite, reveals that the maximum electric field magnitude within the operating band is concentrated at the center of the second (central) GGW cavity. Therefore, a centrally placed corrugated profile is considered for the top lid to mitigate the multipactor effect.

The multipactor performance of this smooth lid GGW filter, already analyzed in [10] at 17.4 GHz, has been computed with different number of corrugations. For the multipactor simulations, the measured SEY values of the aluminum material used in the fabrication of this filter [10] included in Table 2 have been used in this case, in addition to those of the ECSS standard for aluminum, for comparison. To determine the appropriate number of corrugations to include in the top lid of this filter, a parametric study has been again performed to evaluate the influence of the number of corrugations on both the obtained P_{th} and on its RF performance. Table 6 summarizes the obtained P_{th} values for different number of corrugations.

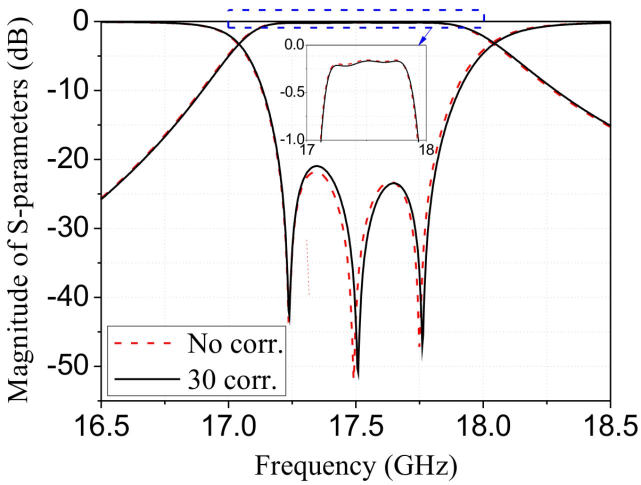

Figure 7: RF performance of the GGW filter with smooth lid and with 30 corrugations.

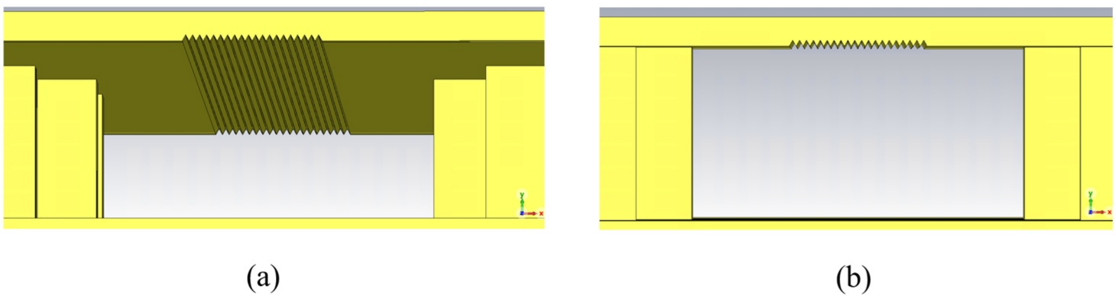

Figure 8: Corrugated top lid for the GGW filter. a) 3D view. (b) Front view.

In addition to the analysis of the obtained P_{th} level, it has been checked that the RF performance of the corrugated-lid GGW filter is not significantly degraded by the insertion of corrugations into its top lid. Once again, in view of the results shown in Fig. 7, which compares the S-parameters of the GGW filter with a smooth lid and the electrical performance of the filter considering the maximum number of corrugations analyzed (30), we can conclude that the introduction of corrugations has only a minor impact on its RF response.

Based on the simulation results and considering the limitations of the available high-power test laboratory, the final design has been implemented with 20 corrugations on the top lid of the GGW structure (see Fig. 8). With this configuration, the simulated P_{th} remains below 6 kW, which corresponds to the maximum power level that can be measured in the intended test facility.

4. Fabrication and Experimental Setup

To verify the simulation results regarding power handling enhancement, multipactor tests must be performed for the proposed designs. Four configurations have been evaluated: the RGW transformer with and without the corrugated surface added to the top lid, and the GGW filter with and without the corresponding corrugated surface profile. The smooth-lid GGW filter and RGW transformer had been previously fabricated using standard CNC milling techniques and measured in the framework of previous works (see [10] and [12]), so only the corresponding corrugated top lids for each component have been newly manufactured, as detailed in section 2. Additional measurements were performed to quantify the manufacturing tolerances and their impact on the geometry. Regarding the corrugations' width, the

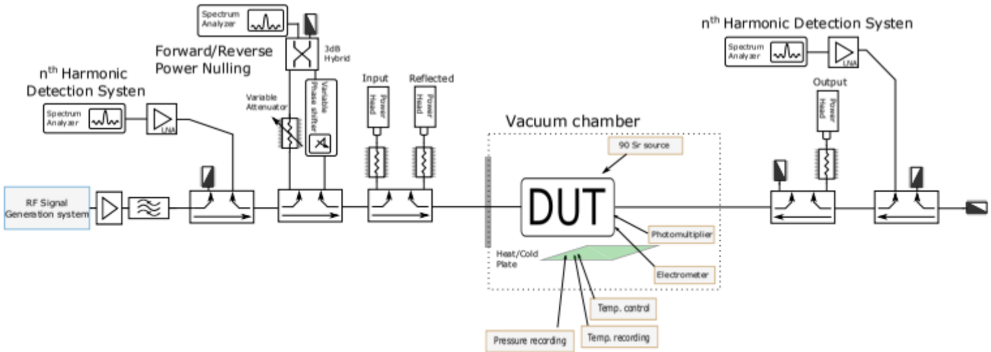

Figure 9: Test bench for MP tests.

nominal design width was 115 μm, while the measured average width is 118 μm, thus obtaining a high degree of precision. A minor asymmetry was observed in the profile, which is a known artifact of the micro-dicing saw process used during machining. On the other hand, the theoretical height was set at 100 μm, and measurements indicate a fabricated height of, approximately, 90 μm. Since the nominal design includes a 3 μm chamfer, the effective target depth is 97 μm. Therefore, the manufacturing error is less than 10 µm, which falls within the acceptable tolerance limits for this fabrication technique. The MP tests were again carried out at the High Power Laboratory of the European Space Agency (ESA) and the Val Space Consortium (VSC) [22], in a class 10,000 (ISO7) certified clean room. The hardware was handled and stored in accordance with flight model precautions.

4.1. Test Setup

The experimental setup used for the MP characterization is shown in Fig. 9. Measurements were conducted using a dedicated Ku-band (WR-51) high-power test facility developed in accordance with the ECSS multipaction test standard [24]. The test bench was capable of delivering up to 6 kW peak RF power at 17 GHz under high-vacuum conditions ($\leq 10^{-5}$ mbar). To simulate the space environment and trigger MP events, a radioactive $Sr^{90}\beta$ source was employed as an electron-seeding mechanism. The source was positioned at the central region of the RGW section and at the central cavity of the GGW filter, where the highest electric-field levels were expected.

To ensure the reliability and repeatability of the measurements, a comprehensive test protocol was implemented, including pre- and post-test vector network analyzer (VNA) characterization of the DUTs, test-bed conditioning, validation, and verification procedures. Prior to DUT testing, the facility was validated using a WR-51 through-waveguide section to confirm discharge-free operation up to the maximum available power at all test frequencies. In addition, the sensitivity of the detection system was verified using a reference sample with a known MP threshold.

During testing, critical parameters including applied and reflected RF power, insertion losses, pressure, and temperature at multiple locations of the DUT were continuously monitored. The maximum measurement uncertainties were ±3.5% for RF power, ±15% for pressure, and ±2 °C for temperature. Multipactor detection was performed using both global and local monitoring techniques. Global methods included forward/reverse power nulling and harmonic detection systems, while local detection relied on electrometers positioned near critical regions of the DUT to monitor electron accumulation, complemented by optical detection techniques.

MP characterization was carried out at 17, 17.4, and 18 GHz using a controlled power-step profile. The RF power was initially set to 570 W and maintained for at least 10 minutes before being progressively increased in steps of approximately 300–400 W up to the maximum available power. The combination of calibrated instrumentation, validated test procedures, and multiple detection techniques provided a high degree of confidence in the accuracy and repeatability of the reported MP threshold measurements. More information on the MP test setup parameters can be found in Table 7.

Table 7
Multipactor test parameters

Parameter	Value
Frequency	17–18 GHz
Max power	6 kW
Pulse length	20 μs
Duty cycle	2%
Pressure	$\leq 10^{-5}$ mbar
Temperature	23°C
Electron source	Sr-90

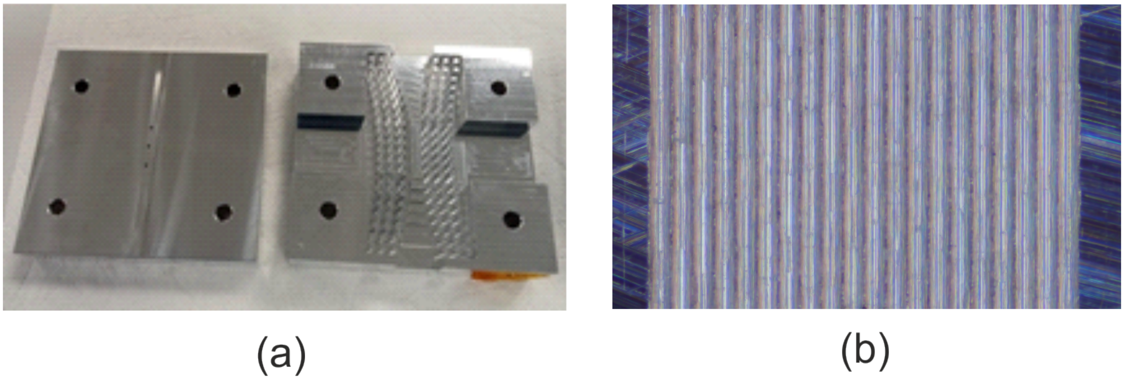

Figure 10: (a) Photograph of the manufactured RGW transformer with its corrugated top lid. (b) Electron microscope image of the corrugated top lid.

5. Measurement Results and Validation

5.1. RGW transformer measurements

A prototype of the corrugated top lid for the RGW transformer with 15 corrugations detailed in section 3.1 has been manufactured in aluminum. A photograph of the RGW transformer with its corrugated top lid can be seen in Fig. 10(a). An electron microscope image of the corrugated top lid is shown in Fig. 10(b), where the implemented corrugation profile can be observed in more detail.

Before MP tests were performed, the scattering parameters of the fabricated device were measured to validate the performance of the fabricated component. Fig. 11 shows the simulated and measured electrical response of the RGW transformer in the frequency range of 15-20 GHz for both configurations (with the smooth top lid, and with the corrugated lid with 15 corrugations). In the figure, dashed curves correspond to simulations, whereas solid curves represent measurements.There is a good correlation between the two sets of data. The RGW transformer has overall good return loss (RL) values. For the smooth lid configuration, the RL stays above 32 dB in the frequency design band (17-18 GHz), while for the corrugated lid configuration, RL above 30 dB is still obtained. With the smooth lid the RL is slightly higher. This behavior is attributed to small manufacturing variations, which are not unusual for these high-frequency components. Nevertheless, the measured insertion loss (IL) for both smooth-lid and corrugated-lid configurations remains below 0.2 dB across the measured frequency range (0.02 dB for the smooth lid case and 0.12 dB for the corrugated lid structure), so it can be concluded that the performance of the manufactured RGW transformer meets the required specifications (in terms of both IL and RL levels) to perform the high-power tests in the selected experimental facility. It is important to note that the measured IL obtained in the corrugated-lid RGW transformer is rather low, confirming its low-loss performance, given that the corrugations performed on the metallic cover, being macroscopic in nature, do not significantly increase the insertion loss, as predicted by EM simulations. This behavior contrasts with that of rough metallic surfaces, which are known to exhibit consistently higher insertion losses.

After validating the electrical performance of the RGW transformer, the MP tests were then conducted. Once all detectors mentioned in section 4.1 were placed correctly, the device went through multipactor tests. Fig. 12(a) shows a photograph of the RGW transformer placed in the vacuum chamber. As mentioned above, for the RGW transformer

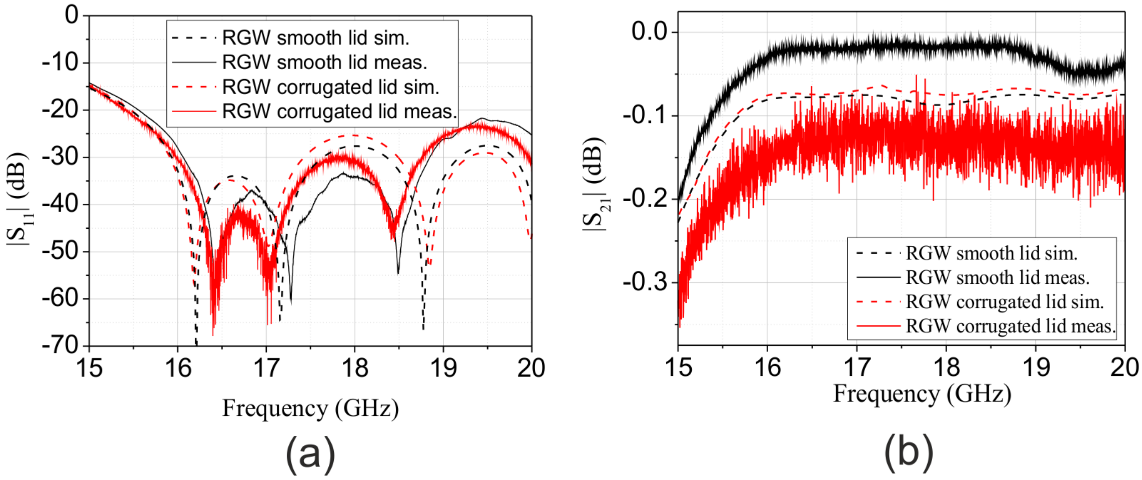

Figure 11: Simulated and measured electrical response of the RGW transformer with smooth and with corrugated top lid. (a) Magnitude (in dB) of the S_{11} parameter. (b) Magnitude (in dB) of the S_{21} parameter.

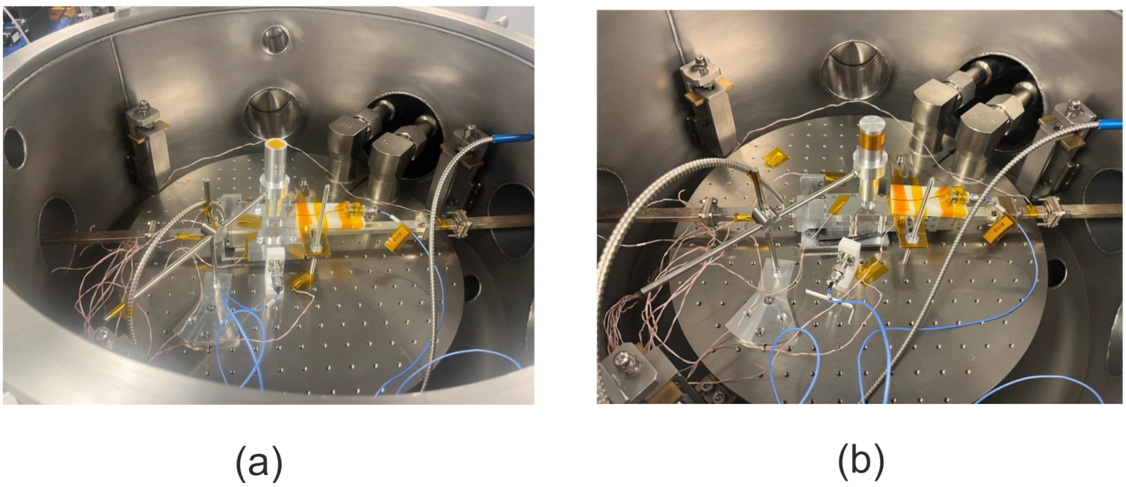

Figure 12: Photographs of the setups in the vacuum chamber for performing the MP tests (a) on the RGW transformer and (b) on the GGW filter.

with smooth and with corrugated lid, three points in the operational frequency range were tested. The P_{th} measured results are included in Table 8 and compared with simulations employing the measured SEY.

There are small discrepancies ranging from 70 W to 470 W between the measured and simulated results. It can also be observed that the measured threshold values are consistently a bit higher than the simulated ones in all cases, which we mainly attribute to SEY uncertainty, as previously observed in other works [12].In this regard, we verified through simulations that slightly reducing the measured SEY values reported in Fig. 3 by only a few hundredths—variations that may arise from aging or surface contamination effects—results in simulated P_{th} values that closely match the experimental measurements.

We can confirm that there is an increase of nearly 2.5 kW at 17 GHz in the P_{th} value of the corrugated-lid RGW transformer. On the other hand, at 17.4 and 18 GHz no MP breakdown was detected for the corrugated design until the maximum achievable power of 6 kW. Thus, we can conclude that, at 17.4 GHz, there has been (at least) an increase in terms of P_{th} of approximately 2 kW, and of more than 1.5 kW at 18 GHz (at least again), with only 15 corrugations

Table 8
Simulated and measured P_{th} values for the RGW transformer

Design	Frequency	Simulation	Measurement
Smooth lid	17 GHz	3593 W	3660 W
	17.4 GHz	3743 W	4035 W
	18 GHz	4056 W	4527 W
Corrugated	17 GHz	5937 W	6150 W
	17.4 GHz	6234 W	P_{th} > 6 kW*
	18 GHz	6812 W	P_{th} > 6 kW*

*No MP breakdown was detected.

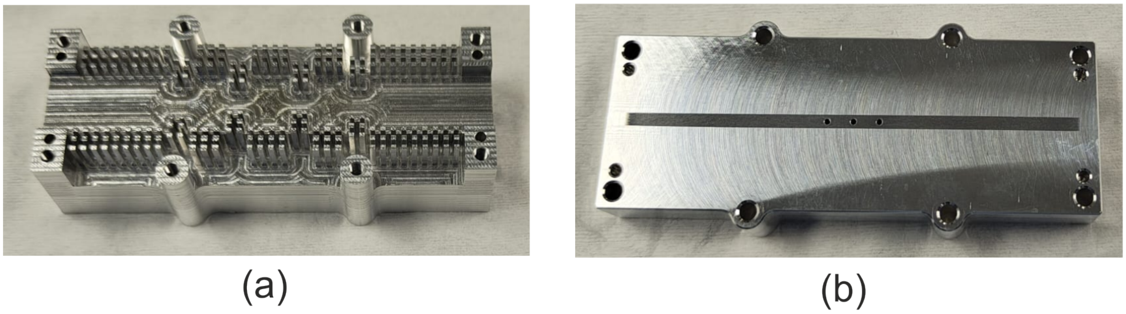

Figure 13: Photograph of (a) the manufactured GGW filter body and (b) its corrugated top lid.

on the top lid of the RGW transformer. These results confirm the predicted improved power-handling capability when using corrugated surface profiles.

5.2. GGW filter Measurements

A corrugated top lid for the GGW filter with 20 corrugations detailed in section 3.2 has been manufactured in aluminum. A photograph of the manufactured filter with the corrugated top lid can be seen in Fig. 13.

Before performing the MP tests, the scattering parameters of the fabricated device were measured to validate the electrical performance of the prototype. The comparison between the simulated and measured responses of the GGW filter prototype is shown in Fig. 14 for both configurations (with the smooth top lid, and with the corrugated lid of 20 corrugations), in the frequency range of 16.5-18.5 GHz. For the smooth-lid component, a comparatively narrower (a difference of about 200 MHz measured transmission band is observed (represented with solid line) reaching the measured insertion loss approximately 0.4–0.5 dB in the midband. The smooth-lid filter response also exhibits a slight frequency shift (approximately 300 MHz) compared to the corresponding simulated response (represented with dashed line), which can be attributed to fabrication tolerances, surface roughness, and assembly misalignment. This can be noted in both the IL and RL. However, RL stays above 20 dB in the frequency range of interest. In contrast, the corrugated-lid configuration demonstrates an even improved measured insertion loss, that remains close to 0.35–0.4 dB across the passband, showing a narrower bandwidth (a similar difference of about 200 MHz), but also a much lower frequency shift in this case (only 30 MHz) with respect to the simulated data, while the measured RL is still higher than 20 dB, confirming the practical utility of the proposed method of insertion of corrugations. In general, the results confirm that the simulations predict well the behavior of the prototype, considering the accuracy level achieved in the manufacturing process.

Following the validation of the GGW filter performance, we proceeded with the multipactor characterization. Once the detector setup described in section 4.1 was finalized, the device underwent rigorous MP testing. Fig. 12(b) shows a photograph of the GGW bandpass filter placed in the vacuum chamber. A second MP campaign was performed on the GGW filter, in this case at a single frequency point of 17.4 GHz. Table 9 summarizes the corresponding simulated and measured multipactor threshold power levels. There are small discrepancies of around 200 W and 400 W between the measured and simulated results. In this case, the measured threshold values are consistently a bit lower than the simulated ones (see Table. 9), which we can again attribute to SEY uncertainty. In this case, we checked through simulations that, slightly increasing the measured SEY values reported in Table. 2 by only a few hundredths, makes

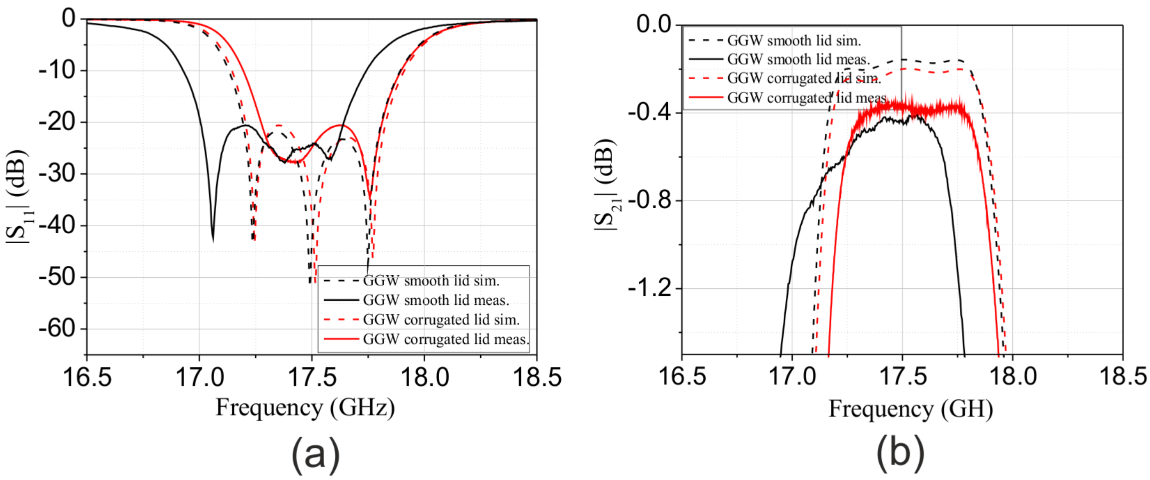

Figure 14: Simulated and measured electrical response of the GGW filter with smooth and with corrugated top lid. (a) Magnitude (in dB) of the S_{11} parameter. (b) Magnitude (in dB) of the S_{21} parameter.

Table 9
Simulated and measured P_{th} values for the GGW filter

Design	Simulation (meas. SEY)	Simulation (ECSS)	Measurement
Smooth lid	3679 W	3164 W	3468 W
Corrugated	5562 W	6047 W	5080 W

that the simulated P_{th} values closely match the experimental measurements even better. Such small SEY variations may arise from aging or surface contamination effects [11]. Therefore, the relatively small discrepancies observed between the simulated and measured P_{th} levels support the validity of the MP setup. Thus, we can confirm that there is an increase of approximately 1.5 kW in the P_{th} level between the smooth and the corrugated-lid GGW filter MP test. This clearly indicates that the introduction of corrugations on the top lid effectively enhances the power-handling capability of the GGW filter, which fully confirms the solution proposed in this work.

6. Conclusions

The main contribution of this work is the application of corrugated profiles for multipactor mitigation, along with its experimental validation using practical RGW and GGW components. This paper demonstrates the effectiveness of corrugated surface profiles as a passive technique for mitigating multipactor discharges in gap waveguide technology. Both RGW and GGW structures were analyzed through simulations, as well as validated experimentally. The obtained results confirm that the introduction of corrugations significantly increases the multipactor threshold power, with improvements of approximately 1.5–2 kW, while preserving the RF performance exhibited by the smooth-lid components. Notably, these improvements were achieved using only a limited number of corrugations placed in the central region of the analyzed structures, reflecting a practical trade-off between electrical performance, manufacturability, and achievable power handling. The good agreement between simulations and measurements validates the employed methodology and confirms the robustness of the proposed solution.

Overall, corrugated surfaces provide a simple, manufacturable, and efficient approach to enhance the power-handling capability of microwave hardware, specifically addressing multipactor breakdown constraints in high-power space applications.

References

[1] M. Jiménez, B. Gimeno, C. Miquel-Espanya, D. Raboso, S. Anza, C. Vicente, J. Gil, F. Quesada, A. Álvarez, M. Taroncher, Analysis of the electromagnetic radiation generated by a multipactor discharge occurring within a microwave passive component, J. Phys. D: Appl. Phys. 43

(2010) 395501.
[2] A. J. Hatch, H. B. Williams, Multipacting modes of high-frequency gaseous breakdown, Physical Review 112 (1958) 681–685.
[3] J. R. M. Vaughan, Multipactor, IEEE Transactions on Electron Devices 35 (1988) 1172–1180.
[4] J. R. M. Vaughan, A new formula for secondary emission yield, IEEE Transactions on Electron Devices 36 (1988) 1963–1967.
[5] A. Wood, J. Petit, Diagnostic investigations into the multipactor effect, susceptibility zone measurements and parameters affecting a discharge, Technical Report, ESA-ESTEC, ESA Publication Division, Noordwijk, The Netherlands, 1989.
[6] W. Tang, C. M. Kudsia, Multipactor breakdown prediction in rectangular waveguide-based components, in: Proceedings of IEEE Conference on Military Communications, Monterey, CA, USA, p. 181–187.
[7] A. Coves, G. Torregrosa-Penalva, C. Vicente, B. Gimeno, V. Boria, Multipactor discharges in parallel-plate dielectric-loaded waveguides including space-charge effects, IEEE Transactions on Electron Devices 55 (2008) 2505–2511.
[8] V. E. Semenov, E. I. Rakova, D. Anderson, M. Lisak, J. Puech, Multipactor in rectangular waveguides, Physics of Plasmas 14 (2007) 033501–1–033501–8.
[9] A. Berenguer, A. Coves, B. Gimeno, E. Bronchalo, V. Boria, Experimental study of the multipactor effect in a partially dielectric-loaded rectangular waveguide, IEEE Microwave and Wireless Components Letters 29 (2019) 595–597.
[10] A. Jorge-Lopez, J. J. Vague, I. Asensio, A. Coves, A. A. San-Blas, M. Baquero-Escudero, M. Taroncher, A. Vidal, V. Boria, Theoretical and experimental results for multipactor effect in groove gap waveguide bandpass filters with inductive coupling irises, IEEE Access 12 (2024) 187844–187856.
[11] F. Kazemi, M. Mostajeran, G. Romanov, Analysis of multipacting threshold sensitivity to the random distributions of the secondary electron yield parameters, Scientific Reports (14, 2024) (2024).
[12] S. M. Bonte, M. Sancho, A. Coves, E. Rajo-Iglesias, J. J. Vague, V. Boria, Study of the multipactor effect in ridge gap waveguide technology, IEEE Transactions on Electron Devices (Early Access, 2026) (2026).
[13] J. J. Vague, I. Asensio, A. Coves, A. A. San Blas, M. Reglero, A. Vidal-Pantaleoni, D. Raboso, M. Baquero-Escudero, V. Boria, Study of the multipactor effect in groove gap waveguide technology, IEEE Transactions on Microwave Theory and Techniques 70 (2022) 2566–2578.
[14] R. L. Ives, C. Oldham, M. Gilmore, I. J. Kern, Performance of multipactor coatings applied using atomic layer deposition, in: IEEE International Conference on Plasma Science (ICOPS), Seattle, WA, USA, pp. 1–1.
[15] D. I. Montero, L. Aguilera, U. Wochner, Antimultipactor device, 2016. Patent WO2016042192A1, WIPO (PCT), US10724141B2, CA2973088C, ES2564054B1.
[16] O. Peverini, G. Addamo, R. Tascone, G. Virone, P. Cecchini, R. Mizzoni, F. Calignano, E. P. Ambrosio, D. Manfredi, P. Fino, Enhanced topology of E-plane resonators for high-power satellite applications, IEEE Transactions on Microwave Theory and Techniques 63 (2015) 3361–3373.
[17] J. Hueso, C. Vicente, B. Gimeno, V. E. Boria, S. Marini, M. Taroncher, Multipactor effect analysis and design rules for wedge-shaped hollow waveguides, IEEE Transactions on Electron Devices 57 (2010) 3508– 3517.
[18] W.-Z. Cui, Y. Li, J. Yang, T.-C. Hu, X.-B. Wang, R. Wang, N. Zhang, H.-T. Zhang, Y.-N. He, An efficient multipaction suppression method in microwave components for space application, Chinese Physics B 25 (2016) 068401.
[19] C. Chang, Y. D. Li, J. Verboncoeur, Y. S. Liu, C. L. Liu, Suppressing double-metal-surface resonant multipactor by three dimensional wavy surface, Physics of Plasmas 24 (2017) 040702.
[20] I. Arregui, F. Teberio, I. Arnedo, A. Lujambio, M. Chudzik, D. Benito, T. Lopetegi, R. Jost, F.-J. Görtz, J. Gil, C. Vicente, B. Gimeno, V. E. Boria, D. Raboso, M. A. G. Laso, High-power low-pass harmonic filters with higher-order TEn0 and non-TEn0 mode suppression: Design method and multipactor characterization, IEEE Transactions on Microwave Theory and Techniques 61 (2013) 4376–4386.
[21] S. Bonte, R. García, A. Coves, J. M. Garcia-Barcelo, A. A. San-Blas, M. Sancho, M. A. Sanchez-Soriano, V. Boria, Study of the insertion of corrugations in microwave filters for mitigation of the multipactor effect, AEU - International Journal of Electronics and Communications 202 (2025) 156036.
[22] Val Space Consortium, European Space Agency (ESA) and Val Space Consortium (VSC) High-Power Laboratories, 2026. Accessed: 2026-04-26.
[23] Dassault Systèmes, SPARK3D CST Studio Suite, 2025.
[24] ESA-ESTEC, ESA Publication Division, Multipacting and Design Test, Technical Report, European Cooperation for Space Standarization (ECSS), Noordwijk, The Netherlands, 2020.